Biochimica et Biophysica Acta 1838 (2014) 3191–3202

Contents lists available at ScienceDirect

Biochimica et Biophysica Acta

journal homepage: www.elsevier.com/locate/bbamem

Two homologous neutrophil serine proteases bind to POPC vesicles with different affinities: When aromatic amino acids matter

Anne-Sophie Schillinger [a,b], Cédric Grauffel [a,b,1], Hanif Muhammad Khan [a,b], Øyvind Halskau [a], Nathalie Reuter [a,b,*]

[a] Department of Molecular Biology, University of Bergen, Pb. 7803, N-5020 Bergen, Norway
[b] Computational Biology Unit, Department of Informatics, University of Bergen, Pb. 7803, N-5020 Bergen, Norway

ARTICLE INFO

Article history:
Received 20 February 2014
Received in revised form 29 August 2014
Accepted 3 September 2014
Available online 16 September 2014

Keywords:
Amphitropic protein
Large unilamellar vesicles
Molecular dynamics simulations
SPR: surface plasmon resonance
Proteinase 3
Neutrophil elastase

ABSTRACT

Neutrophil serine proteases Proteinase 3 (PR3) and human neutrophil elastase (HNE) are homologous antibiotic serine proteases of the polymorphonuclear neutrophils. Despite sharing a 56% sequence identity they have been shown to have different functions and localizations in the neutrophils. In particular, and in contrast to HNE, PR3 has been detected at the outer leaflet of the plasma membrane and its membrane expression is a risk factor in a number of chronic inflammatory diseases. Although a plethora of studies performed in various cell-based assays have been reported, the mechanism by which PR3, and possibly HNE bind to simple membrane models remains unclear. We used surface plasmon resonance (SPR) experiments to measure and compare the affinity of PR3 and HNE for large unilamellar vesicles composed of 1-palmitoyl-2-oleoyl-sn-glycero-3-phosphocholine (POPC). We also conducted 500-nanosecond long molecular dynamics simulations of each enzyme at the surface of a POPC bilayer to map the interactions between proteins and lipids and rationalize the difference in affinity observed in the SPR experiment. We find that PR3 binds strongly to POPC large unilamellar vesicles ($K_d = 9.2 \times 10^{-7}$ M) thanks to the insertion of three phenylalanines, one tryptophan and one leucine beyond the phosphate groups of the POPC lipids. HNE binds in a significantly weaker manner ($K_d > 10^{-5}$ M) making mostly electrostatic interactions via lysines and arginines and inserting only one leucine between the hydrophobic lipid tails. Our results support the early reports that PR3, unlike HNE, is able to directly and strongly anchor directly to the neutrophil membrane.

1. Introduction

Neutrophils are the most abundant type of leukocytes and are key components of the innate immune system, able to mediate both anti-infectious and pro-inflammatory effects [1,2]. Neutrophil serine proteases (NSP) Proteinase 3 (PR3, EC 3.4.21.76) and human neutrophil elastase (HNE) are homologous antibiotic serine proteases of the polymorphonuclear neutrophils (PMNs) which can be considered as important cellular targets in a number of chronic inflammatory diseases [3]. PR3 and HNE are mainly localized within the azurophilic granules of resting neutrophils and can be exposed at the cell surface when the neutrophils are activated. Despite sharing a 56% sequence identity (Fig. 1) and a high structural similarity (Cf. Fig. 2A) [4] PR3 and HNE have been shown to have different functions and localizations in the neutrophils. In particular, and in contrast to HNE, PR3 has been detected in secretory vesicles and on the outer leaflet of the plasma membrane [5,6]. Because of its peculiar localization PR3 has been suggested to play a role in the pathophysiology of various chronic inflammatory diseases involving neutrophils and especially in granulomatosis with polyangeitis, a systemic vasculitis associated with autoantibodies against PR3 [6–10].

Witko-Sarsat et al. first reported a specific association of PR3 to the plasma membrane, which they described as stronger "than only an ionic interaction" [11]. On the other hand Campbell et al. argued in favor of a weak charge-dependent mechanism similar for both

Abbreviations: PR3, proteinase 3; HNE, human neutrophil elastase; LUV, large unilamellar vesicle; POPC, 1-palmitoyl-2-oleoyl-sn-glycero-3-phosphocholine; SPR, surface plasmon resonance; MD, molecular dynamics

* Corresponding author at: University of Bergen, Department of Molecular Biology, Pb. 7803, N-5020 Bergen, Norway. Tel.: +47 555 84040, fax: +47 555 89683.
E-mail addresses: Anne-Sophie.Schillinger@mbi.uib.no (A.-S. Schillinger), cedric@ibms.sinica.edu.tw (C. Grauffel), Hanif.Khan@mbi.uib.no (H.M. Khan), Oyvind.Halskau@mbi.uib.no (Ø. Halskau), nathalie.reuter@mbi.uib.no (N. Reuter).
[1] Present address: For Cédric Grauffel: Institute of Biomedical Sciences, Academia Sinica, Taipei 115, Taiwan.

http://dx.doi.org/10.1016/j.bbamem.2014.09.003
0005-2736/

```
PR3      IVGGHEAQPHSRPYMASLQMRGNPGSHFCGGTLIHPSFVLTAAHCLRDIP  63
HNE      IVGGRRARPHAWPFMVSLQLRG---GHFCGATLIAPNFVMSAAHCVANVN  63
         ****:.*:**: *:*.***:**    .****.*** *.**::****: ::

PR3      QRLVNVVLGAHNVRTQEPTQQHFSVAQVFLNNYDAENKLNDILLIQLSSP 111
HNE      VRAVRVVLGAHNLSRREPTRQVFAVQRIFENGYDPVNLLNDIVILQLNGS 111
         * *.*******:  :***:* *:* ::* *.**. * ****:::**...

PR3      ANLSASVATVQLPQQDQPVPHGTQCLAMGWGRVGAHDPPAQVLQELNVTV 162
HNE      ATINANVQVAQLPAQGRRLGNGVQCLAMGWGLLGRNRGIASVLQELNVTV 162
         *.:.*.* ..*** *.: : :*.******** :* :   *.*********

PR3      VTFFCRPHNICTFVPRRKAGICFGDSGGPLICDGIIQGIDSFVIWGCATR 222
HNE      VTSLCRRSNVCTLVRGRQAGVCFGDSGSPLVCNGLIHGIASFVRGGCASG 222
         ** :**  *:**:*  *:**:******.**:*:*:*:** ***  ***:

PR3      LFPDFFTRVALYVDWIRSTLR 243
HNE      LYPDAFAPVAQFVNWIDSIIQ 243
         *:** *: ** :*:** * ::
```

Fig. 1. Sequence alignment of PR3 and HNE. The two sequences share 56% sequence identity. We use boxes to highlight amino acids of HNE aligning with the predicted PR3 IBS (blue fonts for basic residues and orange for hydrophobic amino acids). Amino acids forming the catalytic triad are labeled with green fonts.

proteases [12]. In agreement with the work of Witko-Sarsat et al., Goldman et al. showed using spectrophotometry techniques that PR3 and HNE bind with different affinities to reconstituted lipid bilayers [13]. Using bilayers with different ratios of zwitterionic (DMPC[2]) and anionic (DMPG[3]) phospholipids, they showed that while PR3 binds to DMPC vesicles with an estimated K_d of 85 μM. HNE wasn't observed to bind to pure DMPC vesicles but binds to mixed DMPC:DMPG 1:1 liposomes with a K_d of 14.5 μM. The authors also show that PR3 binds best to DMPC:DMPG 1:1 vesicles with a K_d of 4.5 μM. Moreover results from differential scanning calorimetry and hydrophobic photolabelling indicate that PR3 inserts amino acids into the hydrophobic region of the lipid vesicles, while HNE does it to a lesser extent. In 2004, Durant et al. used PR3 and HNE cDNA transfected mast cell lines and showed that PR3 was expressed at the cell surface after induced degranulation while HNE was released into the extra-cellular medium. Using molecular dynamics simulations with at first a simple membrane model [14], we have reported that PR3 inserts aromatic and aliphatic amino acids into the hydrophobic core of the bilayer models, while HNE interacts mostly via electrostatic interactions to the bilayer interface. We further used relatively short MD simulations (50 ns) of PR3 with explicit DMPC bilayers to describe the protein–lipid interactions at the atomic level of detail [15]. We reported an interface-binding site (IBS) composed of a few basic amino acids (R177, R186A,[4] R186B, K187, R222) that ensure proper orientation of PR3 towards the membrane to allow for the insertion of a hydrophobic patch (V163, F165, F166, I217, W218, L223, F224) (Fig. 2B). Mutations of four hydrophobic (F165, F166, L223, F224) or four basic amino acids (R186A, R186B, K187, R222) significantly affects the membrane expression of PR3 in a cell-based assay, thus validating the role of the predicted IBS for PR3 membrane expression [16]. Taken altogether these studies indicate that despite their high sequence similarity, PR3 and HNE interact with lipid membranes using different types of interactions. This is further supported by the amino acid substitutions in the region of the PR3 IBS (Cf Fig. 2) where in particular two of the three phenylalanines, as well as tryptophan W218, are substituted by non-aromatic residues in HNE.

The available data to date has been obtained by different teams using a wide range of approaches and models, from cell-based assays to molecular modeling, but only one study using standard biophysics methods in 1999 [13].

It is generally acknowledged that the association of peripheral proteins with lipid bilayers is fast while the dissociation is slow meaning that the dissociation rate constant is the main determinant of the binding strength. As a consequence, in simple systems, the affinity for the membrane is mostly accounted for by interactions between the protein interfacial binding site and lipids. Such interactions can be investigated by molecular dynamics (MD) simulations using the protein of interest docked on an all-atom lipid bilayer; this will provide a detailed map of the lipid–protein interactions, and for example the respective contributions of hydrophobic and polar amino acids (see Refs. [17–19]). Surface plasmon resonance has been successfully used to study interactions between lipid vesicles and proteins and can be used to obtain accurate values of equilibrium dissociation constants (K_d) [20,21]. Both SPR and MD methods are thus complementary as they provide information at different levels of resolution.

We here report a combined in vitro and in silico study investigating the affinity of PR3 and HNE for POPC bilayers. We chose POPC vesicles as the thickness of POPC bilayers is more relevant to model the plasma membrane than those of DMPC. The choice of zwitterionic PC headgroups is relevant to the main lipid constituents of the plasma membrane and allows us to focus on short-range interactions with the bilayers, and in particular on the energetic contribution of the insertion of hydrophobic amino acids. We use SPR to characterize the affinity of PR3 and HNE for large unilamellar vesicles (LUVs) and 500-nanosecond long molecular dynamics simulations of the two enzymes at the surface of a pre-equilibrated POPC bilayer to map the interactions between proteins and lipids at the atomic level of detail. The use of SPR allows us to obtain insights, albeit limited, into the kinetics of PR3 and HNE binding to POPC vesicles.

2. Material and methods

2.1. Molecular modeling

2.1.1. Molecular dynamics simulations

We performed MD simulations of both PR3 and HNE inserted in POPC lipid bilayers using the following procedure: (1) equilibration of the lipid bilayer, (2) insertion of the protein in the lipid bilayer and

[2] DMPC:dimyristoylphosphatidylcholine.
[3] DMPG:dimirystoylphosphatdylglycerol.
[4] We use the chymotrypsin numbering for both PR3 and HNE. It presents the advantage of providing a consistent numbering for all enzymes of the family but introduces letters in addition to the numbering (e.g. the two consecutive arginines labeled as 186A and 186B).

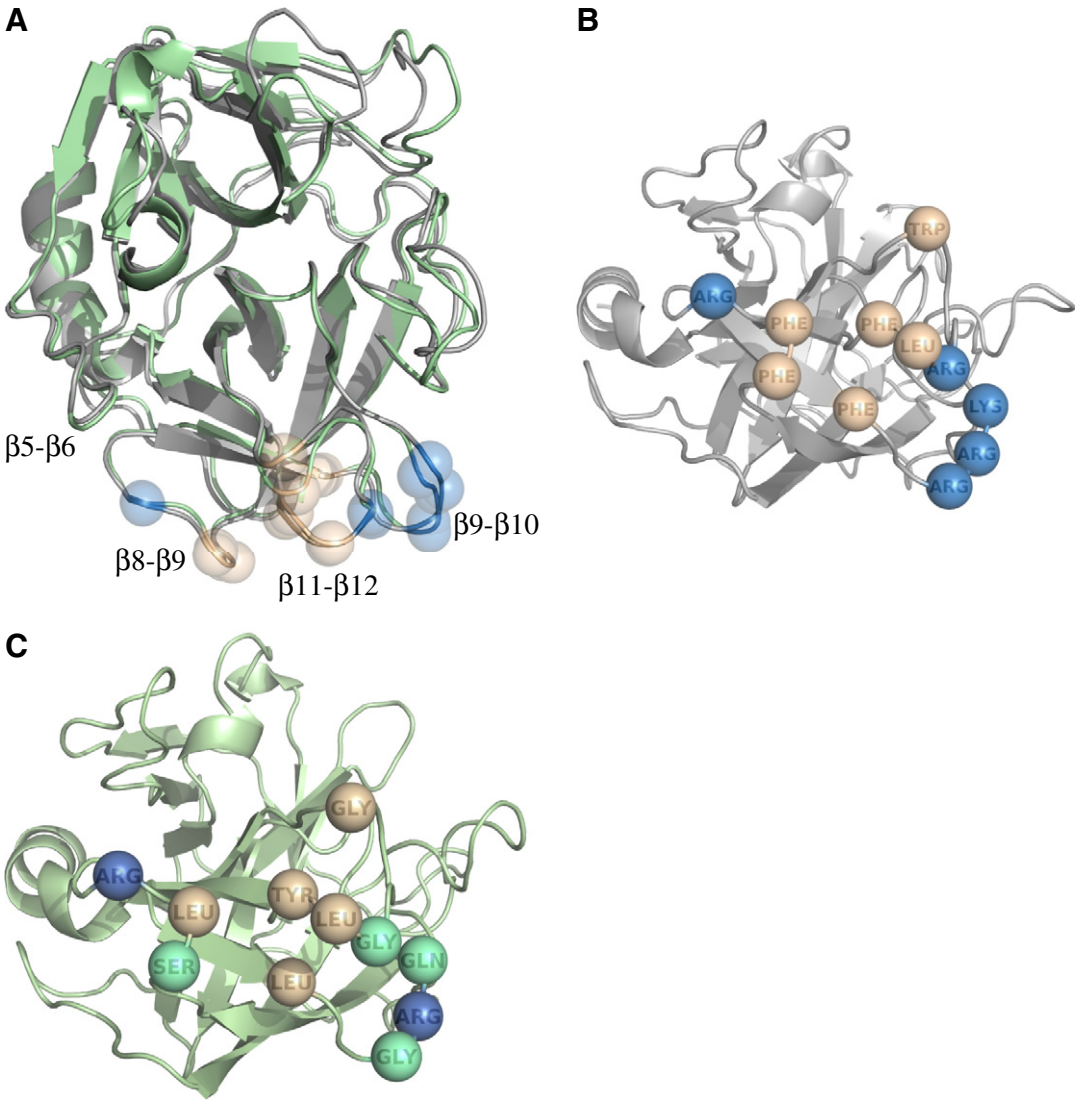

Fig. 2. (A) Structural alignment of PR3 (gray) and HNE (green). The protein secondary structure elements are represented using cartoons while each amino acid forming the PR3 IBS, as well as the amino acids of the HNE sequence aligning with the PR3 IBS (Cf. Fig. 1), are represented using balls (blue and orange for basic and hydrophobic amino acids, respectively, green for others). The nature of these amino acids in PR3 and HNE is shown on panels (B) and (C), respectively.

(3) simulation of the protein-bilayer complex and subsequent analysis of the resulting trajectories (Table 4).

In this manuscript we consequently use the chymotrypsin numbering for both PR3 and HNE. It presents the advantage of providing a consistent numbering for all enzymes of the family but introduces letters in addition to the numbering (e.g. the two consecutive arginines labeled as 186A and 186B).

2.1.1.1. POPC bilayer. A lipid bilayer made of 256 POPC was built using the CHARMM-GUI [22–24]. The lipid bilayer was subjected to energy minimization using NAMD [25] and the CHARMM36 force field update for lipids [26]. The system was then equilibrated without surface tension for 300 ps at 310 K using a time step of 2 fs and velocities reassignment every 500 fs, and subsequently run into production for 80 ns. The SHAKE algorithm was applied to constrain bonds between hydrogen and heavy atoms [27]. Non-bonded interactions were truncated using a cutoff of 12 Å, using a force-based switch function for van der Waals and a shift function for electrostatics. For estimating long-range electrostatic forces, the particle-mesh-Ewald (PME) algorithm was used [28,29]. The Langevin algorithm was used to control temperature (310 K, damping coefficient: 1.0) and pressure (target pressure: 1 atm, oscillation period: 75 fs, oscillation decay time: 25 fs) [30]. The area per lipid and the order parameters were monitored along the simulation to assess the properties of the bilayer. The order parameters S_{CD} were calculated with VMD [31] from the mean value of the angle between each C–H bond of the lipid tails and the normal to the membrane. The profiles are consistent with those in Ref. [26]. The surface area was calculated to be 65.5 ± 0.8 Å^2 on average during the simulation, close to that reported by Klauda et al. [26] (64.7 ± 0.2 Å^2) for a POPC bilayer simulated using the same CHARMM 36 force field. Kučerka et al. report an estimate of 68.3 ± 1.5 Å^2 using hybrid electron density models [32].

2.1.1.2. Insertion of Proteinase 3 and HNE at the interface of the lipid bilayer. The cartesian coordinates of PR3 were taken from chain A of the X-ray structure referenced 1FUJ [33] in the RSCB Protein Data Bank [34] and those of HNE from the 1PPF structure [35]. PR3 and HNE were then oriented with respect to, and inserted at, the interface of the equilibrated POPC lipid bilayer as described previously for PR3 [15]. Briefly, each of the enzymes was positioned at the surface of a POPC lipid bilayer in the orientation predicted by implicit bilayer simulations for HNE [14] and using earlier all-atom simulations with a DMPC bilayer for PR3

Table 1
Anchorage of PR3 in a POPC lipid bilayer: inventory of interactions and depth of anchorage.

Loop	Amino acid	Depth[a] (Å)	Hydrophobic contacts[b]	Hydrogen bonds[c] (%)	Cation–π[e] (%)
β5–β6	K99	−11.2 2.8		20.1	
β8–β9	V163	−3.0 ± 1.9	2.3		
	T164	−2.8 ± 2.0		45.6	
	F165	+ 1.3 ± 1.8	1.5		
	F166	+ 1.7 ± 1.7	2.5	**28.1**	
	R177	−4.8 ± 2.5	1.1	87.9	
β9–β10	R186A	+ 0.0 ± 2.3	4.2	85.9	
	R186B	−2.2 ± 2.7	1.5	58.7[d]/82.9	
	K187	−1.2 ± 2.4	1.6	**90.4**/74.5	
β11–β12	F215	−10.0 ± 2.2			5.9
	W218	+ 0.8 ± 2.8	1.9	**26.6**	5.7
	T221	−0.9 ± 2.4	1.6		
	R222	−0.2 ± 2.0		49.0[d]	
	L223	+ 2.5 ± 2.2	5.8		
	F224	+ 0.3 ± 1.8	1.2		
	P225	−2.0 ± 1.6	1.9		

[a] Positive values indicate that the center of mass of the amino acid is buried in the bilayer beyond the plane defined by the phosphate groups.
[b] Average number of hydrophobic contacts per frame (listed if above 1).
[c] Occupancies of hydrogen bonds with POPC phosphate groups in % (if >20; bold numbers are for hydrogen bonds involving the protein backbone).
[d] Hydrogen bond between Arg186B or Arg222 and POPC glycerols.
[e] Occupancy of cation–π adducts (if >5%).

[15]. PR3 was then translated 2 Å above its initial position to account for the difference in width between POPC and DMPC bilayers. Six lipids overlapping with the proteins were removed, in both the cases of PR3 and HNE and as reported earlier for phosphatidylinositol specific phospholipase C [36]. The starting conformation for HNE is shown on Fig. 3A, the starting conformation of PR3 is not represented but displays a depth of anchorage similar to that of HNE.

2.1.1.3. Simulations PR3-POPC and HNE-POPC. The systems were then minimized with CHARMM (v33b1) [37] using the following harmonic restraints: 150 kcal/mol/Å^2 on the protein backbone, water and ion molecules, 100 kcal/mol/Å^2 for membrane located further than 5 Å and 75 kcal/mol/Å^2 less than 5 Å from the protein and 10 kcal/mol/Å^2 for protein side chains located at a distance of 5 Å or less from the membrane. The minimization consisted of 20 cycles of 500 steps of steepest descent and 100 steps of conjugate gradients algorithms with restraints being scaled by 0.65 after each cycle. The systems were then solvated in a cubic box of TIP3 water molecules [38] using VMD (version 1.8.7) [31]. Two and eleven chloride ions were added by replacing random water molecules to neutralize the system for PR3 and HNE, respectively. The system was subsequently equilibrated using NAMD [25] and the CHARMM force field (c22 with CMAP corrections [39]) with two short runs of 400 ps in NVT ensemble, with velocities reassigned every 50 fs and 500 fs, and then further equilibrated for 2 ns. The integration of the equations of motion was done using a Multiple Time Step algorithm [40]; bonded interactions and short-range nonbonded forces were evaluated in every step and long range electrostatics every second step. The system was then run into production for 500 ns in the NPT ensemble. Pressure and temperature control, as well as the cutoff scheme and treatment of long-range electrostatic interactions are the same as for the equilibration of the bilayer.

Table 2
Anchorage of HNE in a POPC lipid bilayer: inventory of interactions and depth of anchorage.

Loop	Amino acid	Depth[a] (Å)	Hydrophobic contacts[b]	Hydrogen bonds[c] (%)	Cation-π[e] (%)
β5–β6	P96	−7.2 ± 5.8	1.0		
	V97	−3.8 ± 5.3	2.6		
β7–β8	R146	−9.4 ± 2.5		69.0	
β8–β9	T164	−5.7 ± 2.7		25.8	
	S165	−2.9 ± 2.5		36.0	
	L166	−0.6 ± 2.1	5.9	25.4	
	R177	−4.3 ± 3.1	1.1	64.8	
	R178	−4.3 ± 3.2		**23.2**/84.9	
β9–β10	R186	−6.7 ± 3.8		62.2/20.2[d]	
	G186A	−6.9 ± 3.5		**41.7**	
	F192	−11.6 ± 3.8			13.2
β11–β12	R217	−7.2 ± 4.4		49.0	
	S221	−3.2 ± 2.4		28.0	
	G222	−2.6 ± 2.1		**28.4**	
	L223	+0.4 ± 2.0	6.3		
	Y224	−1.3 ± 1.9		31.1[d]	

[a] Mean values and standard deviations. Positive values indicate that the center of mass of the amino acid is buried in the bilayer beyond the plane defined by the phosphate groups.
[b] Average number of hydrophobic contacts per frame (listed if above 1).
[c] Occupancies of hydrogen bonds in % (occupancies less than 20% are omitted; bold numbers for backbone hydrogen bonds).
[d] Hydrogen bond between R186 or Y224 and POPC glycerols.
[e] Occupancy of cation–π adducts (occupancies less than 5% are omitted).

Table 3
LUV immobilization levels and chip coverage accession by BSA binding (BSA is used at 0.1 mg/ml and is injected 60 s at 10 μl · min^{-1}). Values reported are the means and standard deviations of four experiments.

Immobilization level (RU)	BSA binding level (RU)
8669 ± 95	43 ± 2.6

2.1.1.4. Analysis. Based on the evolution of the root mean square deviation (RMSD) between the trajectory conformations and the conformation of the enzymes before the MD simulations (Cf. supplementary data, Fig. S1), we decided to use the trajectories between 200 and 500 ns as sampling windows. All analyses are thus performed on the last 300 ns of the simulations.

The occupancies of hydrogen bonds were calculated with the CHARMM program [37] using a 2.4 Å cutoff distance between hydrogen and acceptor and a 130° donor–hydrogen–acceptor angle criterion. The donor and acceptor definition are taken from the CHARMM force field [38]. Hydrophobic contacts were defined using a 3 Å cutoff distance between aliphatic groups of the lipids and of the enzymes (Charmm atom types ca; cb; cg1; cg2; cg2; ha*; hb*; hg; hg2*; type cg except for hsd, hse, asn, asp; type hg1 except for cys, thr, ser; type cd except for arg, gln, glu; type cd1; type cd2 except for hsd, hse; type ce1, ce2, cz and associated hydrogens of phe, tyr, type cd1, cd2, ce2, ce3, cz2, cz3 and associated hydrogen of trp, type cay and type hy*). Cation–π interactions between aromatic rings (phenylalanine, tyrosine and tryptophan) are considered to exist when all distances between the heavy atoms of the aromatic ring and choline nitrogen are below 7 Å and when these distances do not differ by more than 1.5 Å [41,42].

We evaluated the depth of anchorage of the proteins as described in Grauffel et al. [36]. Briefly we used the mean z coordinate of the phosphorus atoms as a reference plane. The center of mass of each residue was calculated and its difference to the reference plane was calculated. The corman module of the Charmm program was used for coordinate statistics. Values reported are means of the distances of the last 300 ns of simulations. Averaged electron density profiles (EDP) were calculated using the VMD Density Profile plugin [43], at 0.5 Å resolution using a structure per nanosecond (on sampling window). Residue profiles were normalized with respect to the peak of the phosphate profile.

Table 4
K_d values for PR3 and HNE with POPC LUVs. Values reported are the means and standard deviations of six experiments for PR3 and four for HNE.

K_d (×10^{-7} M)	
PR3	HNE
9.22 ± 0.4	>100

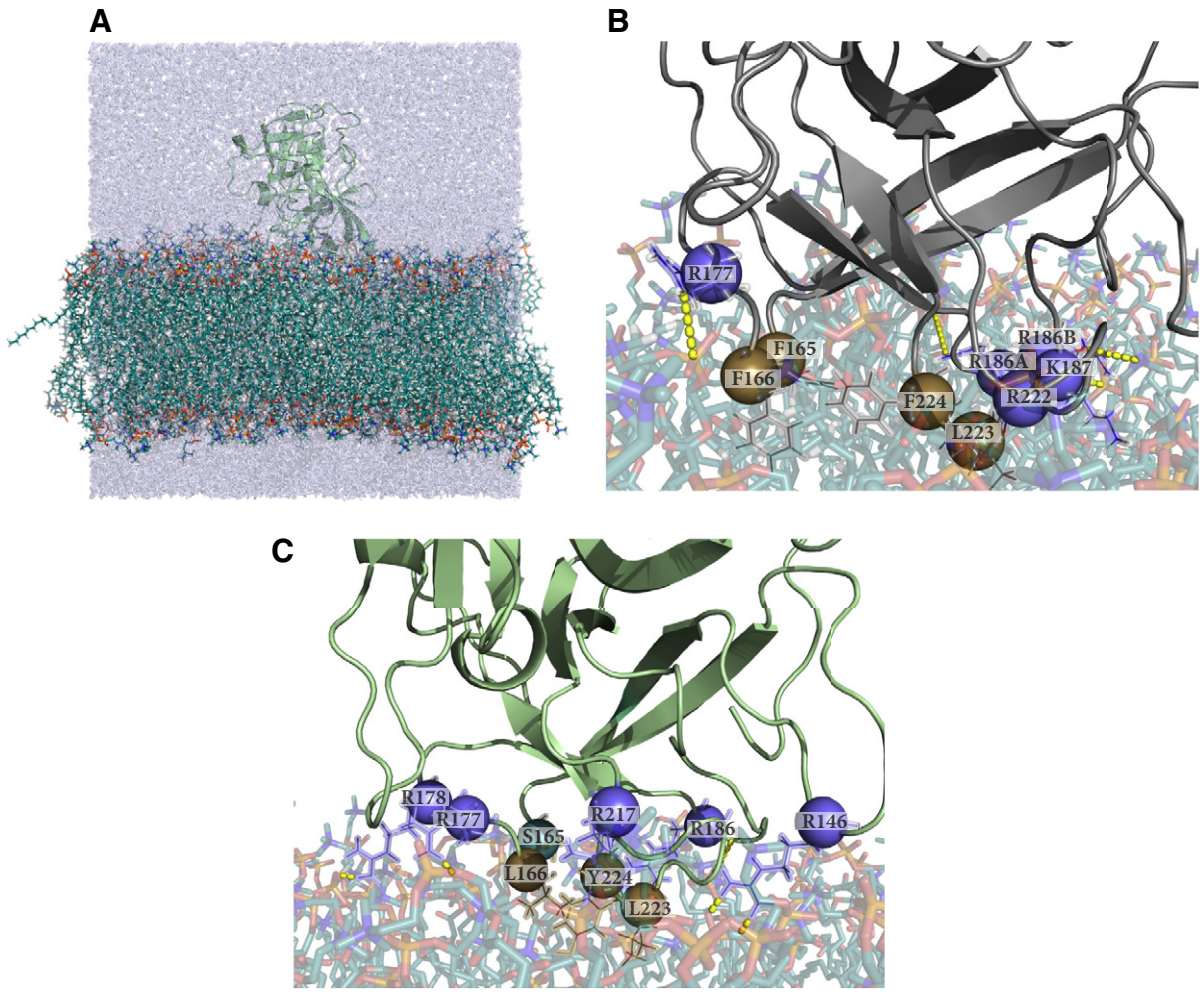

Fig. 3. Molecular dynamics simulations of PR3 and HNE at the surface of a POPC bilayer. (A) Simulated system with HNE represented using green cartoons, the POPC bilayer using sticks colored by atom types and the water molecules in light blue. Randomly picked snapshots of (B) PR3 and (C) HNE interface binding sites (at 286 and 343 ns, respectively). Amino acids mediating either hydrogen bonds of at least 45% occupancy for hydrogen bonds or at least one hydrophobic contact on average, are highlighted with balls. Yellow dashed lines represent hydrogen bonds.

2.1.2. Energetic contributions to membrane binding using IMM1

We used the IMM1 membrane model [44], as implemented in Charmm [37] (v38) to evaluate the binding energy of PR3 and HNE to a zwitterionic membrane as a function of their distance to the membrane. IMM1 is based on the EEF1 model for water-soluble proteins, which uses a linear distance-dependent dielectric constant, neutralizes the ionic side chains, and adds a Gaussian solvent exclusion term to the CHARMM 19 energy function [45]. In IMM1 the membrane is represented as a hydrophobic slab. The solvation parameters change smoothly from aqueous values outside the membrane to values corresponding to a nonpolar solvent inside the membrane. Briefly, the effective energy of the protein is given by:

$$W_{IMM1} = E_{intra} + \Delta G_{solv} \quad (1)$$

where E_{intra} is the intramolecular energy of the protein given by the CHARMM 19 and ΔG_{solv} its solvation free energy calculated as described in Ref. [44].

We calculated W_{IMM1} of the protein anchored at the membrane [14] and then every angstrom along an axis parallel to the membrane normal, up to a distance of 15 Å above the membrane plane; the distance is defined by the shortest distance between protein and membrane surface. The starting geometries are chosen as the bound structures from earlier IMM1 simulations [14] and are kept rigid during the procedure. The binding energy of PR3 (and HNE) to membranes could thus be calculated as the difference between the effective energy with the membrane model IMM1 and the effective energy in water (EEF1.1), which was also calculated:

$$\Delta W_{IMM1} = \Delta E_{intra} + \Delta\Delta G_{solv} \quad (2)$$

The total binding energy ΔW_{IMM1} of each of the proteins can be decomposed into terms that represent the contribution of each type of atom to the change in solvation energy plus the electrostatic term:

$$\Delta W_{IMM1} = \Delta E_{elec} + \Delta W_{hydrophobic} + \Delta W_{polar} \quad (3)$$

ΔE_{elec} is the change in the intra-molecular coulombic term when transferring the protein from water to the membrane. Since the same structure is used to calculate W_{IMM1} (water) and W_{IMM1} (membrane) the bonded terms and the van der Waals contribution cancel out. The next two terms represent the contribution to $\Delta\Delta G_{solv}$ (Eq. (3)); $\Delta W_{hydrophobic}$ is the contribution from the aromatic groups (atoms of type CR* in Charmm19) and the aliphatic groups (CH* atom types in Charmm 19) and ΔW_{polar} is the contribution from the polar groups.

2.2. Sample preparation

2.2.1. Proteins

PR3 and HNE were purchased from Athens Research & Technology and fatty acid free bovine serum albumine (BSA) from Sigma. According to the manufacturer, the purity of PR3 and HNE is higher than 95%. We assessed it using SDS-page and also have assessed the enzyme activity of the enzymes in kinetic assays.

2.2.2. Liposomes

The lipids (POPC) were purchased from Avanti Polar Lipids. Liposomes were prepared as reported in [46]. Lipids solvated in chloroform were added in glass tubes in the prerequisite amount. Lipids were handled and kept out of light and reactive atmosphere as much as possible by operation in hoods, flushing reagent bottles with dry N_2, and using glass containers wrapped in aluminum foil. The chloroform solutions were dried under dry N_2 pressure. Traces of chloroform were removed by subjecting the samples to vacuum for at least 2 h. Lipid cakes were rehydrated with HBS-N buffer (HBS-N: 0.100 mM HEPES, 150 mM NaCl, pH 7.4) and vortexed vigorously until all films were suspended as slurry. For liposome-preparation, solutions were subjected to seven freeze–thaw cycles using liquid N_2 and a water bath. The hydrated multilamellar structures were then extruded at room temperature and well above the lipid T_m using a Mini-Extruder (Avanti Polar Lipids) assembled using two Millipore filters of 100 nm pore size. Samples were forced through the filters 10 times using Hamilton syringes and the resulting solutions were transferred to clean, foil wrapped glass tubes and stored at 4 °C. Final liposome composition was 100% POPC and the total lipid concentration was 2.5 mM.

2.3. Surface plasmon resonance

The SPR analyses were carried out on a BIAcore T200 (BIAcore, GE Healthcare) and Biacore T200 Control Software. All experiments were carried at 25 °C. Protein and lipid interactions were monitored using a L1 sensor chip. A preparation procedure was performed before each experiment. The surface of the L1 sensor chip was first cleaned with a 1 min injection of 40 mM octylglucoside at a flow rate of 10 μL/min. Liposome solutions were diluted to 1 mM concentration with running buffer and injected at a flow rate of 1 μL/min for 10 min until maximum binding was reached. Liposome maximum deposition was about 8500 response units (RU) for POPC. The surface of the L1 chip was then washed with a solution of 10 mM NaOH for 1 min at a flow rate of 10 μL/min. The completeness of the chip coverage was assessed by injection of bovine serum albumin (BSA) at 0.1 mg/mL and at a rate of 10 μL/min for 60 s. Generally this injection did not perturb the lipid-covered chip by more than 43 RU, and it rapidly fell back to its original value when injection of BSA stopped. Binding assays were then performed on the validated chips. The two proteins (PR3 and HNE) were diluted to sets of at least 5 different concentrations ranging from 0.125 μM to 3 μM (0.125, 0.5, 1, 2, 3) for PR3 (two additional concentrations for HNE, 6 and 9 μM), and were injected over the immobilized liposomes at a flow rate of 5 μL/min for 120 s and 180 s (for HNE and PR3 respectively) until equilibrium was reached. The dissociation phase was measured for at least 420 s after the addition of the sample. At the end of the binding assay, the surface of the sensor chip was regenerated with a solution of octylglucoside 40 mM for 30 s at a flow rate of 30 μL/min. No reference channel was used due to non-specific binding of PR3 on the chip [47]. Instead we focused on achieving maximal coverage of the chip with liposomes and in this way ensure that the resulting SPR signal was completely dominated by the protein interacting with the lipid membrane [48]. The SPR data were analyzed with the Biacore T200 Evaluation Software. Binding affinities were calculated using the steady state affinity model (Langmuir model) and maximal resonance unit (RU) was plotted against concentration. Additional experiments were performed at increasing salt concentrations to evaluate its effect on the binding of PR3 and HNE. We measured the binding responses of PR3 and HNE (0.5 μM) with [NaCl] = 150 mM, [NaCl] = 300 mM and [NaCl] = 700 mM.

3. Results

3.1. Molecular modeling

3.1.1. Molecular dynamics simulation with an explicit bilayer model

PR3 and HNE were positioned at the interfacial region of POPC lipid bilayers as described in the Material and methods section and illustrated on Fig. 3A. Each system was simulated for 500 ns and analyzed in order to characterize the interactions between the enzyme interfacial binding sites and the lipids. We report in Tables 1 and 2 the occupancy of significant hydrogen bonds along the sampling window (occupancy above 20%), as well as the average number of hydrophobic contacts for the amino acids that achieve on average more than one contact per frame of the trajectory. On Fig. 3 we show a snapshot of the simulations of PR3 (Fig. 3B) and HNE (Fig. 3C).

3.1.1.1. PR3. The simulation indicates that the structure of PR3 is not affected by the presence of the membrane; the average RMSD between the conformations in the trajectory is 1.54 ± 0.19 Å on the sampling window (Cf Fig. S1, Supplementary Data). PR3 remains at a stable depth of anchorage at the bilayer interface; we calculate a distance of 19.7 ± 1.6 Å between the center of mass of PR3 and the average plane of the phosphorus atoms (Cf. Supplementary Data, Fig. S2). Interactions between PR3 and the POPC bilayer are mediated almost exclusively by amino acids located on three different loops: β8–β9 (amino acids 163 to 180), β9–β10 (184–197), β11–β12 (215–225). The positions of PR3 amino acids with respect to the average plane of the phosphorus atoms gives an indication of their depth of anchorage in the lipid bilayer. Two loops are anchored significantly beyond the phosphorus atoms; loop β11–β12 appears to be the one that has the deepest anchorage. The β8–β9 loop with F165 and F166 is also anchored beyond the plane of the phosphorus atoms. Yet the average depths of anchorage measured are not characteristic of deep anchoring, and suggest a positioning of the loops at the interface. The β9–β10 loop carries most of the basic cluster identified in our early implicit membrane simulations [14] and is positioned slightly above the two other ones.

Most of the hydrogen bonds we observe involve the phosphate groups of POPC lipids. A low number of hydrogen bonds with occupancies below 20% involve glycerol groups, only Arg186B[5] (58.7%) and Arg222 (49.0%) have occupancies of hydrogen bonds with glycerol above 20% indicating that they are buried somewhat deeper in the interface than the other basic amino acids. The strongest hydrogen bonds involve basic amino acids (R177, R186A, R186B and K187) and have occupancies above 80%. Remarkably Lys187 is involved in hydrogen bonds through its side chain (74.5%) and backbone (90.4%). We have earlier predicted, using simulations with an implicit membrane model and mutagenesis experiments [16], that R186A, R186B, K187 and R222 play a major role in PR3 interaction with cell membranes. In particular mutating these four amino acids into four alanines would abrogate PR3 membrane expression in Rat Basophil Leukemia (RBL) cells. Our results confirm the importance of this cluster of basic amino acids constituted of four arginines (R177, R186A, R186B, R222) and one lysine (K187). Besides these, lysine 99 (K99) reported to be important for ligand binding [49,50] mediates hydrogen bonds with the lipids. It is also the case of F166 and W218 although they mediate interactions via their backbone atoms while their side chains are heavily involved in hydrophobic contacts with the lipid tails.

[5] PR3 and HNE amino acids are numbered according to the chymotrypsin convention, which is common for all serine proteases of the family. To account for insertions this convention includes letters and numbers (Cf Materials and methods section).

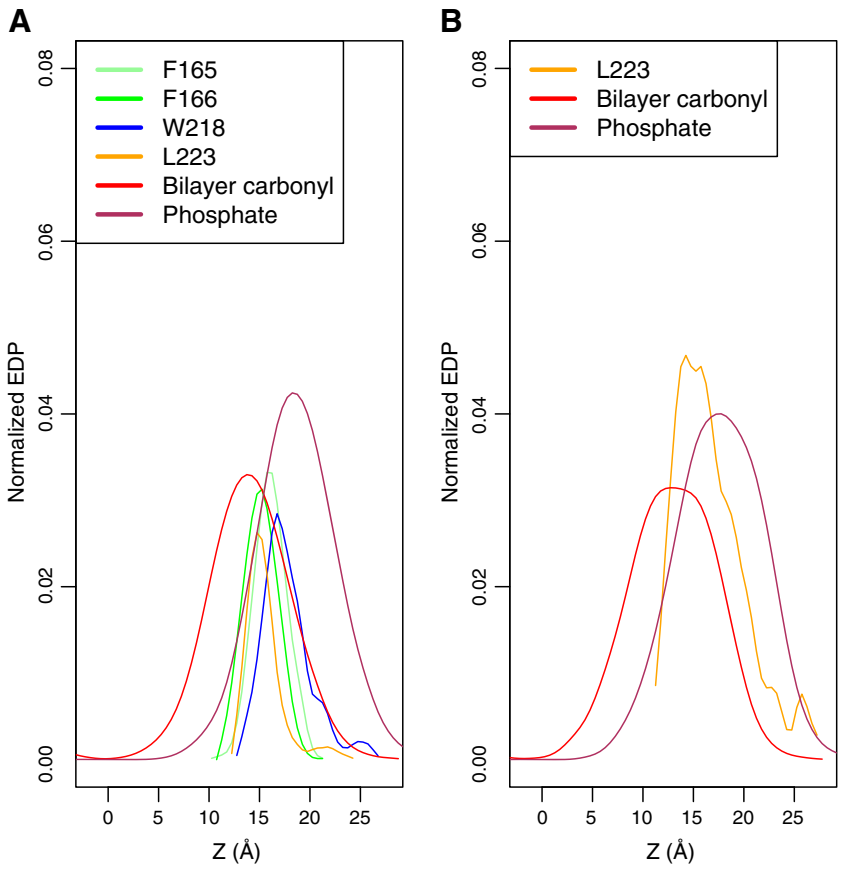

Fig. 4. PR3 and HNE hydrophobic amino acid anchoring. Normalized electron density profiles (EDP) for selected amino acids (F165, F166, W218, and L223 for PR3, L223 for HNE) calculated from the MD simulations of (A) PR3 and (B) HNE. EDPs of the carbonyl (C atom) and phosphate groups (phosphorus atoms) are also plotted. EDPs are averaged over the last 300 ns of the simulations during which the penetration of the above-mentioned amino acids remains unchanged.

We calculated the average number of hydrophobic contacts per frame along the sampling window (Cf. Table 1). Several amino acids of the predicted interfacial binding site display hydrophobic contacts with the POPC lipid bilayer. As expected these are aromatic (F165, F166, W218, F224) and hydrophobic amino acids (V163, T221, L223 and P225). Among these, V163, F166, L223 have particularly high average number of contacts (2.3, 2.5 and 5.8, respectively). Yet their anchorage is not very deep within the hydrophobic tails but rather at the lowest level of the interfacial region. Indeed the density profiles (Fig. 4A) show expected values for F165, F166 and L223 at 15.7, 15.2 and 15.2 Å, respectively. These are between the expected values for the phosphates ($z = 18.2$ Å) and the carbonyl groups ($z = 13.7$ Å). The positioning of the phenylalanine is comparable to previously reported anchorage of phenylalanines of Osh4 [18]. Simultaneous mutations of the four amino acids F165, F166, L223 and F224 did impair membrane expression of PR3 on RBL cells [16]. Interestingly the basic cluster involved in strong hydrogen bonding (R177, R186A, R186B, K187) is also involved in hydrophobic contacts with the lipid tails. In agreement with its involvement in hydrogen bonds with POPC glycerol groups, R186A is the basic amino acid with the higher number of hydrophobic contacts. The aromatic residues F165, F166, W218 and F224 are actually embedded in the bilayer.

While we observed strong cation–pi interactions between W218 and DMPC lipids in our previous work, the occupancy of this interaction is of only 5.7% in the present simulation, which we do not consider as being significant.

3.1.1.2. HNE. Using an implicit membrane model, we previously predicted that HNE would bind to cell membranes using the same interfacial binding site as PR3 [14]. We therefore inserted HNE in the POPC bilayer similarly to Proteinase 3; using the same orientation and the same depth of anchoring. With the implicit membrane model, we also observed a higher electrostatic contribution than in the case of PR3 and fewer contributions from hydrophobic amino acids.

The structure of HNE is unaffected by the POPC bilayer (RMSD 1.26 ± 0.17 Å) and as PR3, it remains stably anchored at the bilayer interface (Cf. Supp Mat, Fig. S2) although a visual inspection of the trajectories indicate that the orientation of HNE with respect to the membrane plane varies more than that of PR3. Most of the interactions with POPC lipids are achieved by amino acids carried by the same three loops as in PR3 (β8–β9, β9–β10, β11–β12) (Cf Table 2) plus an additional interaction through R146 (loop β7–β8). In fact basic residues located on the loops β7–β8, β8–β9 and β9–β10 seem to alternate as anchors with the protein tilting around an axis perpendicular to the bilayer along the simulation. This is well illustrated by the variation along time of the depth of anchoring of amino acids R146 (β7–β8), R177, R178 (β8–β9) and R186 of loop β9–β10 (Cf Fig. S3 in Supplementary data). The proline and valine numbered 96 and 97, respectively (P96, V97, on loop β5–β6), are involved in interactions with the lipid tails as illustrated by their number of hydrophobic contacts (1.0 and 2.6, respectively. Cf Table 2). V97 is only two amino acids away from L99, which interestingly is not observed to interact with the lipids. Its equivalent in PR3 is a lysine (K99) and is observed to interact with the lipid heads via hydrogen bonds.

Hydrogen bonds between HNE and the lipids are mediated by more amino acids than in the case of PR3 (12 against 8) but only one out of the twelve, R178, has an occupancy above 80%. R177 and R178 are the arginines that on average are the most deeply inserted into the interface during the simulation (Cf Table 2 and Fig. S3 in supplementary data). Of the basic amino acids involved in hydrogen bonds with lipids, only

R177 is also involved in the PR3 IBS (Cf. Fig. 1 and Table 1). Yet HNE achieves a high number of hydrogen bonds with lipids when positioned on the bilayer surface, using other arginines not conserved in PR3 (R146, R178, R186, R217).

Only five amino acids mediate an average number of hydrophobic contacts above or equal to 1.0 (V97, P96, L166, R177 and L223). This is strikingly less than in PR3 for which 12 amino acids had a higher number of hydrophobic contacts than this threshold. The two leucines mediate the highest number of contacts and L223 is the only residue anchored beyond the phosphate plane (Cf Table 2). The electron density profile of L223 shows an anchorage comparable to that observed for PR3 (CF. Fig. 4B), between the carbonyl and phosphate groups, with an expected anchorage value of z = 14.2 Å. Carbonyl and phosphate groups have expected values of 13.2 Å and 17.7 Å, respectively. Amino acid K99 of PR3 forms hydrogen bonds with POPC lipids (Cf previous paragraph), while it is not the case of its equivalent in HNE (L99) which cannot form hydrogen bonds; instead two other amino acids of the same loop (β5–β6, P96 and V97) mediate hydrophobic contacts with the lipids.

All together the simulation results indicate that HNE interacts with the bilayer using mostly hydrogen bonds and very few hydrophobic anchors, suggesting a looser binding to lipid membranes than PR3.

3.1.2. Energetic contribution of hydrophobic amino acids to membrane binding

Using an implicit membrane model, we could estimate the contribution of hydrophobic amino acids to the binding energy of PR3 and HNE. These contributions, as well as the total binding energy are plotted on Fig. 5 for distances between the membrane and the proteins ranging from the protein being anchored to a distance of 15 Å between the protein and the membrane surface. Both PR3 (Fig. 5A) and HNE (Fig. 5B) show comparable unfavorable contributions (ca. 5 kcal/mol) from the sum of their polar amino acids and the intra-molecular electrostatics term (Cf Material and methods section). The contribution from aliphatic and aromatic residues, on the other hand, is significantly larger for PR3 (−9 kcal/mol) than for HNE (at most −4 kcal/mol) when the proteins are anchored. This results in an overall favorable binding of PR3 with an optimum energy of ca. −4.5 kcal/mol and a slightly unfavorable binding energy for HNE. The resolution of the model we used and the fact that we used a rigid protein do not allow us to obtain accurate evaluation of the total binding energy and in particular of the short-range interactions that are dependent on atomic level of description. The HNE binding energy could still be slightly favorable albeit far from being as favorable as the one from PR3. Overall these values indicate that the affinity of PR3 for zwitterionic membranes is strongly dominated by its hydrophobic amino acids.

3.2. Surface plasmon resonance

To experimentally verify the hypotheses resulting from the MD simulations, we conducted SPR assays to compare the affinity of PR3 and HNE for large unilamellar vesicles (LUVs) constituted of POPC lipids (Table 3).

3.2.1. Liposome immobilization

Liposomes were immobilized on the surface of the L1 sensor chip at a low flow rate (1 μL · min^{-1}) until the maximal amount of deposition was reached. Liposome immobilization levels were monitored over time and the mean immobilization level for POPC LUVs was 8669 ± 95 RU calculated on four different experiments (Cf. Table 1). To avoid non-specific binding of proteins to the surface of the L1 chips, special care was taken to cover the chip surface at the highest possible levels of liposomes. The level of the coverage sensor chip was assessed with BSA injections (0.1 mg · mL^{-1}). Resulting signals from BSA of around

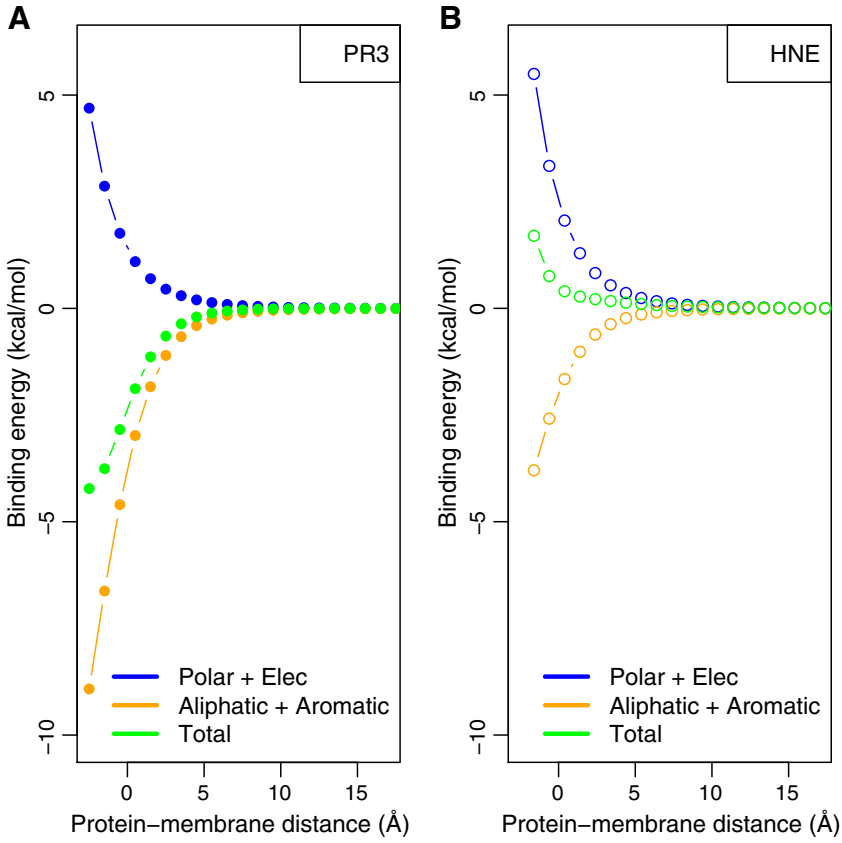

Fig. 5. Hydrophobic and electrostatic contributions to the binding energy of PR3 (A) and HNE (B). The contributions from polar amino acids and intra-molecular electrostatics are plotted in blue, the contribution from aromatic and aliphatic amino acids in orange and the total energy in green.

100 RU or less indicate a sufficient coverage [51]. In our case, BSA binding amounts to 43 ± 2 RUs and allowed us to pursue experiments further with POPC.

3.2.2. Binding of PR3 to POPC LUVs

We investigated the interaction of PR3 with neutral liposomes made of POPC using SPR. Liposomes were immobilized on the surface of the L1 sensor chip as described above. Binding assays were performed by injecting protein samples at increasing concentrations and affinity calculations were carried out by steady state analysis. We monitored the association phase for 180 s and the dissociation phase for 420 s. The sensorgrams (Fig. 6) show that the protein response is concentration dependent and is reaching equilibrium towards the end of each injection. The calculated K_d between PR3 and POPC is 9.22×10^{-7} M. During the dissociation phase, we also observed that the response signal of PR3 does not return to zero and thus demonstrates a persistent binding of PR3 to the liposomes.

3.2.3. Binding of HNE to POPC LUVs

The binding of HNE towards POPC was monitored using the same procedure as for PR3, but using a higher maximum concentration (9 μM). The association of the protein to the LUVs was monitored for 120 s (shorter than for PR3) and the dissociation for 420 s. The sensorgrams are presented on Fig. 6B and show that HNE can bind to liposomes made of POPC in a concentration-dependent manner which indicates a direct binding of the protein to the liposomes. During the dissociation phase, the signal drops immediately and returns to the baseline value. This is in contrast to the behavior of PR3. The kinetics of the protein–membrane interaction seems to be different for the two proteins. For the K_d calculation, the data collected for HNE clearly show that equilibrium was not reached even at an enzyme concentration of 9 μM. It was therefore not possible to calculate the affinity accurately but we can evaluate a lower limit for the K_d value of 1×10^{-5} M.

3.2.4. Effect of salt on HNE and PR3 binding to POPC LUVs

Comparison of binding responses of PR3 and HNE at different salt concentrations (Fig. 7) shows that, at 300 mM NaCl concentration in the running buffer, the PR3 response is less altered than that of HNE as it maintains a rather high binding response. HNE response, however, is considerably lowered compared to the one at [NaCl] = 150 mM. In addition, HNE seems to partially dissociate before the end of the 120 s of injection, indicating a rather unstable binding and difficulties maintain the protein on the lipid vesicles. At 700 mM of NaCl, about a third of the PR3 response is maintained, whereas the binding of HNE is practically abolished.

4. Discussion and conclusion

The SPR experiments yield a K_d in the low micromolar range ($9.22 \pm 0.4 \times 10^{-7}$ M) for PR3, while the binding of HNE is weaker and its K_d is not within the range of concentrations tested; we estimate it to be above 10^{-5} M. For comparison, K_d measured for hIIa-PLA_2 with the same method was $6.8\ 10^{-8}$ M [20] and for the lactadehrin C2 domain $3.2\ 10^{-7}$ M [21]. The difference we observe between PR3 and HNE is consistent with the results of Goldman et al. although we measure a K_d for PR3 with POPC that is lower by two orders of magnitude than the value they determined in 1999 (85×10^{-6} M) using spectrophotometric measurements and DMPC vesicles. This indicates that PR3 binds best to bilayers of unsaturated lipids suggesting that it is sensitive to lipid packing. The study from Goldman et al. appears to have been conducted using multilamellar vesicles, whereas ours were extruded to produce monodisperse unilamellar vesicles.

Although the use of a low flow rate for the injection of protein on the SPR chip prevents us from determining accurate rate constants, the SPR sensorgrams show significantly different dissociation rates for PR3 and HNE, indicating that both enzymes are bound differently to the lipid bilayer with PR3 binding being perpetuated after the flow is interrupted, while HNE transfers back to the bulk almost immediately. Generally, long-range non-specific interactions (typically electrostatics) accelerate the association of peripheral membrane proteins and short range interactions (typically van der Waals) slow the dissociation [52]. While our SPR sensorgrams show no visible differences in the association phase, they show a slower dissociation for PR3, which would therefore imply that short-range interactions are fewer or weaker in HNE. The

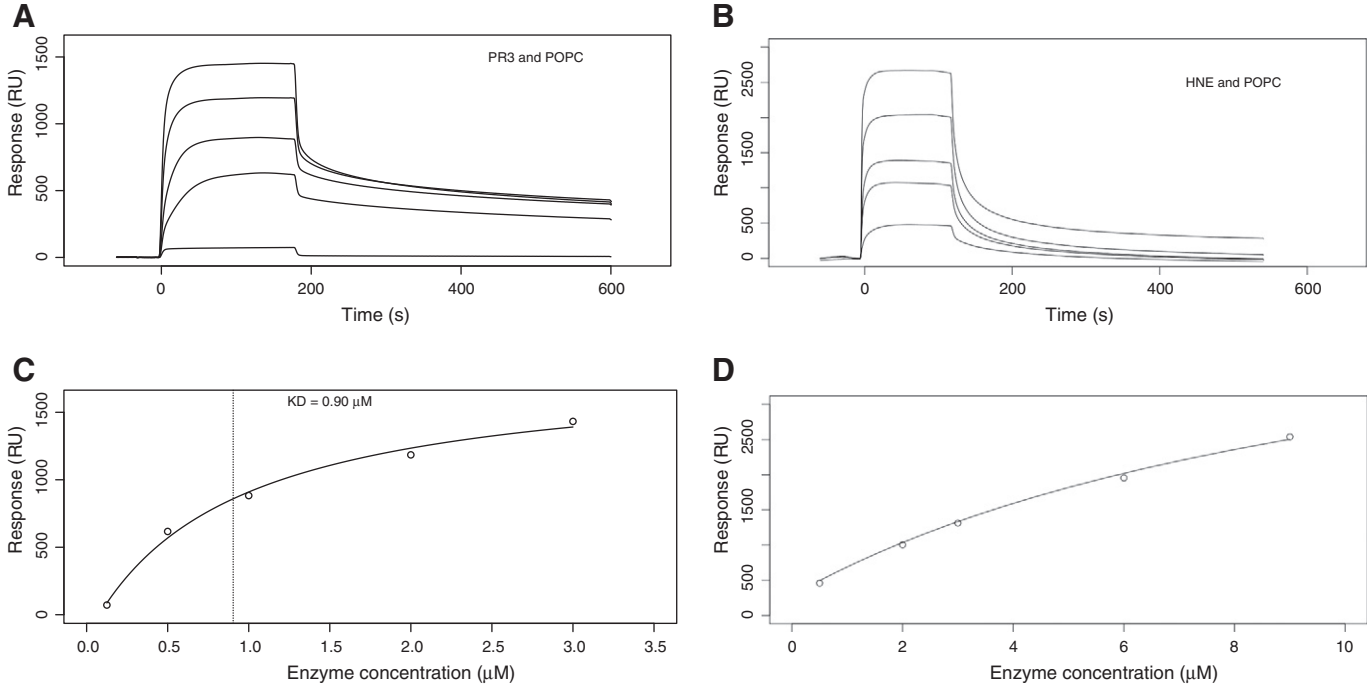

Fig. 6. Binding assay of PR3 and HNE to LUVs from surface plasmon resonance. PR3 (A) and HNE (B) binding responses, and respective affinity data below (C. PR3 and D. HNE) over immobilized POPC. All data are blank subtracted. No double referencing has been done due to high non-specific binding to the reference channel (L1 chip with no liposomes—data not shown).

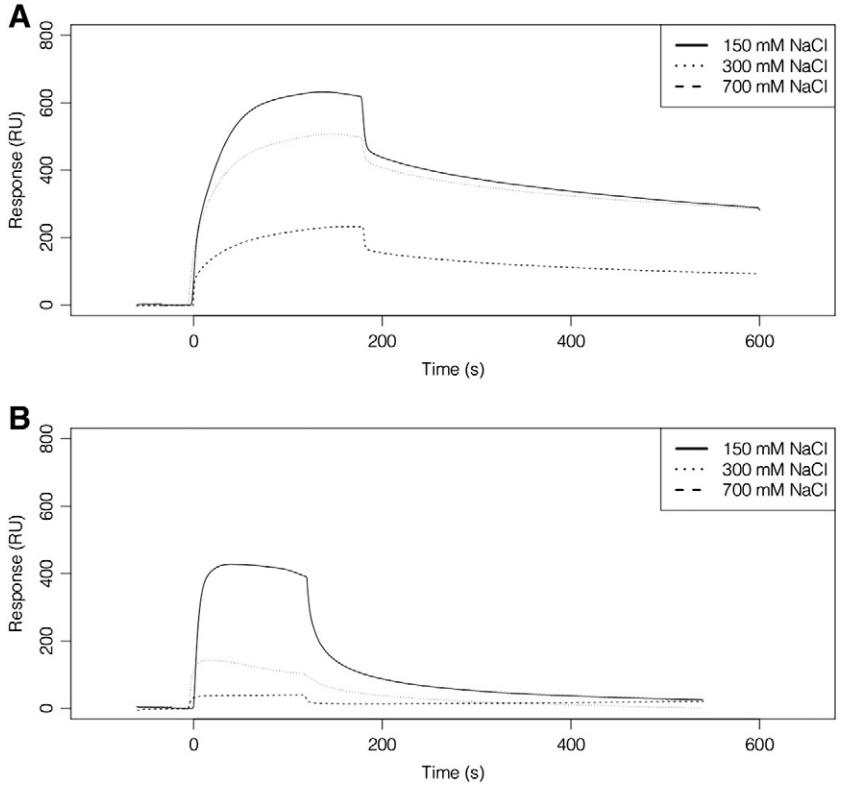

Fig. 7. Binding assay of PR3 (A) and HNE (B) to LUVs from surface plasmon resonance at salt concentrations ranging from 150 mM to 700 mM.

difference between PR3 and HNE in terms of short-range van der Waals interactions is clearly characterized by our MD simulations. The IBS for HNE and PR3 are different (Tables 1 and 2, Fig. 3) leading to a higher average number of hydrophobic contacts per simulation frame between the lipids and PR3 (27.1) than between the lipids and HNE (16.9). On the other hand, and although both HNE and PR3 have about the same number of basic amino acids at their IBS, HNE achieves a higher number of hydrogen bonds with the lipid phosphates. Particularly relevant to the difference in dissociation rates is the fact that PR3 inserts a higher number of aromatic amino acids (F165, F166, W218, F224 in PR3 vs. F192 in HNE) below the plane of the phosphorus atoms. This may also explain the higher shift in the membrane transition temperature observed for PR3 vs HNE by differential scanning calorimetry in the study from Goldman et al. According to the Wimley–White interfacial hydrophobicity scale, based on the transfer free energy of pentapeptides (AcWL–X–LL) from water to a POPC bilayer [53,54], aromatic residues have the most favorable partitioning energies, while charged amino acids have large unfavourable energies. Other amino acids make relatively small contributions. The difference in the number of aromatic residues inserted by both enzymes in the bilayer thus explains the difference in membrane affinity for PR3 and HNE. Anchorage of hydrophobic aromatic residues for anchoring into lipid bilayers has been reported for other amphitropic proteins or peptides [18,55].

The SPR sensorgrams and the difference in the number of hydrophobic and aromatic amino acids anchored in the hydrophobic region of the bilayer between both enzymes is thus consistent with a specific association of PR3 to the plasma membrane, "stronger than only an ionic interaction" [11] with insertion of hydrophobic amino acids [14] while HNE has a more shallow interaction based on hydrogen bonds and short-range electrostatic interactions with LUVs. A qualitative interpretation of SPR measurements using different concentrations of salt (NaCl) shows key differences in the way the binding responses of PR3 and HNE are affected. Whereas PR3 displays a slowly decreasing binding at increasing concentrations of salt, HNE is rapidly and dramatically affected to become nearly abrogated at high salt concentration.

As PR3 is known to bind to the exoplasmic side of the neutrophils plasma membrane, the choice of POPC for the lipid vesicles was motivated by their thickness, closer to plasma membranes than DMPC lipids. Moreover the PC headgroups are relevant with lipid components of the plasma membrane [56–58]. Conveniently the use of vesicles constituted of zwitterionic lipids only allows us to distinguish between the effect of long-range electrostatics and short-range amino acid–lipid interactions. Our results show that PR3 is able to bind to pure PC vesicles, indicating that it could bind to PC domains at the plasma membrane. We expect that adding a fraction of anionic lipids in the bilayer would improve the electrostatic interaction between the lipids and the enzyme in a roughly comparable manner, with a slight advantage for HNE. Yet, and because of its ability to insert 5 hydrophobic amino acids into the lipid bilayer against one for HNE, we would expect PR3 to still be a stronger membrane binder than HNE on membranes containing a fraction of anionic lipids. Studies using vesicles with some anionic lipid content will need to be used to investigate this aspect.

A number of proteins have been shown to be co-localized or co-immunoprecipitate with membrane-expressed PR3 and have been proposed as partners of PR3 at the neutrophil membrane (reviewed in refs [9,59]): CD177 (NB1) [59,60], Fcgamma receptor FcγRIIIb and $p22^{phox}$ subunit of cytochrome b558 [61], β2 integrin adhesion molecule CD11b/CD18 [62], Protease Activated Receptor 2 (PAR2) [63,64], CD177 [65], Phospholipid Scramblase 1 [66] and calreticulin [67]. Yet, to our knowledge, there exist little evidence of a physical interaction between membrane-bound PR3 and the identified partners, except for calreticulin for which a nanomolar affinity has has been reported using SPR experiments. Direct interaction of PR3 with the membrane phospholipids and interaction with protein partners are not mutually exclusive if we consider the formation of a protein complex. Interactions of membrane-bound PR3 with proteins, possibly transmembrane receptors, are indeed necessary for the function of PR3 and would stabilize its interactions with the membrane.

To summarize, using long molecular dynamics simulations of PR3 at the surface of POPC bilayers and SPR experiments following the binding of PR3 to POPC LUVS, we have demonstrated that PR3 can bind directly to POPC lipid bilayers by inserting one aliphatic and four aromatic amino acids into the hydrophobic core of the bilayer. Our results thus indicate that PR3 is able to mediate direct interactions with the exoplasmic leaflet of the neutrophil membrane, which is mostly constituted of PC lipids. HNE interacts with the same LUVs in a shallower manner dominated by short-range electrostatic interactions. The difference in affinity between the two proteins can be explained by the difference in the nature of their IBS, namely the number of hydrophobic aromatic amino acids present.

Acknowledgements

This work was supported by grants from the Bergen Research Foundation and the Norwegian Research Council (FRIMEDBIO #214167). Parallab (High Performance Computing Laboratory at the University of Bergen) and NOTUR (Norwegian metacenter for computational science) are thankfully acknowledged for the provision of CPU time.

Appendix A. Supplementary data

Supplementary data to this article can be found online at http://dx.doi.org/10.1016/j.bbamem.2014.09.003.

References

[1] C. Nathan, Neutrophils and immunity: challenges and opportunities, Nat. Rev. Immunol. 6 (2006) 173–182.
[2] B. Amulic, C. Cazalet, G.L. Hayes, K.D. Metzler, A. Zychlinsky, Neutrophil function: from mechanisms to disease, Annu. Rev. Immunol. 30 (2012) 459–489.
[3] B. Korkmaz, M.S. Horwitz, D.E. Jenne, F. Gauthier, Neutrophil elastase, proteinase 3, and cathepsin G as therapeutic targets in human diseases, Pharmacol. Rev. 62 (2010) 726–759.
[4] E. Hajjar, T. Broemstrup, C. Kantari, V. Witko-Sarsat, N. Reuter, Structures of human proteinase 3 and neutrophil elastase—so similar yet so different, FEBS J. 277 (2010) 2238–2254.
[5] E. Csernok, M. Ernst, W. Schmitt, D.F. Bainton, W.L. Gross, Activated neutrophils express proteinase 3 on their plasma membrane in vitro and in vivo, Clin. Exp. Immunol. 95 (1994) 244–250.
[6] V. Witko-Sarsat, P. Lesavre, S. Lopez, G. Bessou, C. Hieblot, B. Prum, L.H. Noel, L. Guillevin, P. Ravaud, I. Sermet-Gaudelus, J. Timsit, J.P. Grunfeld, L. Halbwachs-Mecarelli, A large subset of neutrophils expressing membrane proteinase 3 is a risk factor for vasculitis and rheumatoid arthritis, J. Am. Soc. Nephrol. 10 (1999) 1224–1233.
[7] A.A. Rarok, C.A. Stegeman, P.C. Limburg, C.G. Kallenberg, Neutrophil membrane expression of proteinase 3 (PR3) is related to relapse in PR3-ANCA-associated vasculitis, J. Am. Soc. Nephrol. 13 (2002) 2232–2238.
[8] A. Schreiber, A. Busjahn, F.C. Luft, R. Kettritz, Membrane expression of proteinase 3 is genetically determined, J. Am. Soc. Nephrol. 14 (2003) 68–75.
[9] V. Witko-Sarsat, N. Reuter, L. Mouthon, Interaction of proteinase 3 with its associated partners: implications in the pathogenesis of Wegener's granulomatosis, Curr. Opin. Rheumatol. 22 (2010) 1–7.
[10] A. Schreiber, F.C. Luft, R. Kettritz, Membrane proteinase 3 expression and ANCA-induced neutrophil activation, Kidney Int. 65 (2004) 2172–2183.
[11] V. Witko-Sarsat, E.M. Cramer, C. Hieblot, J. Guichard, P. Nusbaum, S. Lopez, P. Lesavre, L. Halbwachs-Mecarelli, Presence of proteinase 3 in secretory vesicles: evidence of a novel, highly mobilizable intracellular pool distinct from azurophil granules, Blood 94 (1999) 2487–2496.
[12] E.J. Campbell, M.A. Campbell, C.A. Owen, Bioactive proteinase 3 on the cell surface of human neutrophils: quantification, catalytic activity, and susceptibility to inhibition, J. Immunol. 165 (2000) 3366–3374.
[13] W.H. Goldmann, J.L. Niles, M.A. Arnaout, Interaction of purified human proteinase 3 (PR3) with reconstituted lipid bilayers, Eur. J. Biochem. 261 (1999) 155–162.
[14] E. Hajjar, M. Mihajlovic, V. Witko-Sarsat, T. Lazaridis, N. Reuter, Computational prediction of the binding site of proteinase 3 to the plasma membrane, Proteins 71 (2008) 1655–1669.
[15] T. Broemstrup, N. Reuter, How does proteinase 3 interact with lipid bilayers? Phys. Chem. Chem. Phys. 12 (2010) 7487–7496.
[16] C. Kantari, A. Millet, J. Gabillet, E. Hajjar, T. Broemstrup, P. Pluta, N. Reuter, V. Witko-Sarsat, Molecular analysis of the membrane insertion domain of proteinase 3, the Wegener's autoantigen, in RBL cells: implication for its pathogenic activity, J. Leukoc. Biol. 90 (2011) 941–950.
[17] S. Jaud, D.J. Tobias, J.J. Falke, S.H. White, Self-induced docking site of a deeply embedded peripheral membrane protein, Biophys. J. 92 (2007) 517–524.
[18] B. Rogaski, J.B. Klauda, Membrane-binding mechanism of a peripheral membrane protein through microsecond molecular dynamics simulations, J. Mol. Biol. 423 (2012) 847–861.
[19] C.N. Lumb, J. He, Y. Xue, P.J. Stansfeld, R.V. Stahelin, T.G. Kutateladze, M.S. Sansom, Biophysical and computational studies of membrane penetration by the GRP1 pleckstrin homology domain, Structure 19 (2011) 1338–1346.
[20] R. Stahelin, W. Cho, Differential roles of ionic, aliphatic, and aromatic residues in membrane–protein interactions: a surface plasmon resonance study on phospholipases A2, Biochemistry 40 (2001) 4672–4678.
[21] R.V. Stahelin, Surface plasmon resonance: a useful technique for cell biologists to characterize biomolecular interactions, Mol. Biol. Cell 24 (2013) 883–886.
[22] S. Jo, T. Kim, W. Im, Automated builder and database of protein/membrane complexes for molecular dynamics simulations, PLoS ONE 2 (2007) e880.
[23] S. Jo, T. Kim, V.G. Iyer, W. Im, CHARMM-GUI: a web-based graphical user interface for CHARMM, J. Comput. Chem. 29 (2008) 1859–1865.
[24] S. Jo, J.B. Lim, J.B. Klauda, W. Im, CHARMM-GUI membrane builder for mixed bilayers and its application to yeast membranes, Biophys. J. 97 (2009) 50–58.
[25] J.C. Phillips, R. Braun, W. Wang, J. Gumbart, E. Tajkhorshid, E. Villa, C. Chipot, R.D. Skeel, L. Kale, K. Schulten, Scalable molecular dynamics with NAMD, J. Comput. Chem. 26 (2005) 1781–1802.
[26] J.B. Klauda, R.M. Venable, J.A. Freites, J.W. O'Connor, D.J. Tobias, C. Mondragon-Ramirez, I. Vorobyov, A.D. MacKerell Jr., R.W. Pastor, Update of the CHARMM all-atom additive force field for lipids: validation on six lipid types, J. Phys. Chem. B 114 (2010) 7830–7843.
[27] H.C. Andersen, Rattle—a velocity version of the shake algorithm for molecular-dynamics calculations, J. Comp. Physiol. 52 (1983) 24–34.
[28] T. Darden, D. York, L. Pedersen, Particle mesh Ewald—an N. Log(N) method for Ewald sums in large systems, J. Chem. Phys. 98 (1993) 10089–10092.
[29] U. Essmann, L. Perera, M.L. Berkowitz, T. Darden, H. Lee, L.G. Pedersen, A smooth particle mesh Ewald method, J. Chem. Phys. 103 (1995) 8577–8593.
[30] S.E. Feller, Y.H. Zhang, R.W. Pastor, B.R. Brooks, Constant-pressure molecular-dynamics simulation—the Langevin piston method, J. Chem. Phys. 103 (1995) 4613–4621.
[31] W. Humphrey, A. Dalke, K. Schulten, VMD—visual molecular dynamics, J. Mol. Graph. 14 (1996) 33–38.
[32] N. Kucerka, S. Tristram-Nagle, J.F. Nagle, Structure of fully hydrated fluid phase lipid bilayers with monounsaturated chains, J. Membr. Biol. 208 (2005) 193–202.
[33] M. Fujinaga, M.M. Chernaia, R. Halenbeck, K. Koths, M.N. James, The crystal structure of PR3, a neutrophil serine proteinase antigen of Wegener's granulomatosis antibodies, J. Mol. Biol. 261 (1996) 267–278.
[34] H.M. Berman, J. Westbrook, Z. Feng, G. Gilliland, T.N. Bhat, H. Weissig, I.N. Shindyalov, P.E. Bourne, The protein data bank, Nucleic Acids Res. 28 (2000) 235–242.
[35] W. Bode, A. Wei, R. Huber, E. Meyer, J. Travis, S. Neumann, X-ray crystal structure of the complex of human leukocyte elastase (PMN elastase) and the third domain of the turkey ovomucoid inhibitor, EMBO J. 5 (1986) 2453–2458.
[36] C. Grauffel, B. Yang, T. He, M.F. Roberts, A. Gershenson, N. Reuter, Cation-pi interactions as lipid-specific anchors for phosphatidylinositol-specific phospholipase C, J. Am. Chem. Soc. 135 (2013) 5740–5750.
[37] B.R. Brooks, C.L. Brooks III, A.D. Mackerell Jr., L. Nilsson, R.J. Petrella, B. Roux, Y. Won, G. Archontis, C. Bartels, S. Boresch, A. Caflisch, L. Caves, Q. Cui, A.R. Dinner, M. Feig, S. Fischer, J. Gao, M. Hodoscek, W. Im, K. Kuczera, T. Lazaridis, J. Ma, V. Ovchinnikov, E. Paci, R.W. Pastor, C.B. Post, J.Z. Pu, M. Schaefer, B. Tidor, R.M. Venable, H.L. Woodcock, X. Wu, W. Yang, D.M. York, M. Karplus, CHARMM: the biomolecular simulation program, J. Comput. Chem. 30 (2009) 1545–1614.
[38] A.D. MacKerell, D. Bashford, M. Bellott, R.L. Dunbrack, J.D. Evanseck, M.J. Field, S. Fischer, J. Gao, H. Guo, S. Ha, D. Joseph-McCarthy, L. Kuchnir, K. Kuczera, F.T.K. Lau, C. Mattos, S. Michnick, T. Ngo, D.T. Nguyen, B. Prodhom, W.E. Reiher, B. Roux, M. Schlenkrich, J.C. Smith, R. Stote, J. Straub, M. Watanabe, J. Wiorkiewicz-Kuczera, D. Yin, M. Karplus, All-atom empirical potential for molecular modeling and dynamics studies of proteins, J. Phys. Chem. B 102 (1998) 3586–3616.
[39] A.D. Mackerell, M. Feig, C.L. Brooks, Extending the treatment of backbone energetics in protein force fields: limitations of gas-phase quantum mechanics in reproducing protein conformational distributions in molecular dynamics simulations, J. Comput. Chem. 25 (2004) 1400–1415.
[40] J.A. Izaguirre, S. Reich, R.D. Skeel, Longer time steps for molecular dynamics, J. Chem. Phys. 110 (1999) 9853–9864.
[41] H. Minoux, C. Chipot, Cation–pi interactions in proteins: can simple models provide an accurate description? J. Am. Chem. Soc. 121 (1999) 10366–10372.
[42] F.N.R. Petersen, M.O. Jensen, C.H. Nielsen, Interfacial tryptophan residues: a role for the cation–pi effect? Biophys. J. 89 (2005) 3985–3996.
[43] T. Giorgino, Computing 1-D atomic densities in macromolecular simulations: the density profile tool for VMD, Comput. Phys. Commun. 185 (2014) 317–322.
[44] T. Lazaridis, Effective energy function for proteins in lipid membranes, Proteins 52 (2003) 176–192.
[45] E. Neria, S. Fischer, M. Karplus, Simulation of activation free energies in molecular systems, J. Chem. Phys. 105 (1996) 1902–1921.
[46] O. Halskau, M. Ying, A. Baumann, R. Kleppe, D. Rodriguez-Larrea, B. Almas, J. Haavik, A. Martinez, Three-way interaction between 14-3-3 proteins, the N-terminal region of tyrosine hydroxylase, and negatively charged membranes, J. Biol. Chem. 284 (2009) 32758–32769.
[47] R. Mouri, K. Konoki, N. Matsumori, T. Oishi, M. Murata, Complex formation of amphotericin B in sterol-containing membranes as evidenced by surface plasmon resonance, Biochemistry 47 (2008) 7807–7815.
[48] A. Olaru, M. Gheorghiu, S. David, C. Polonschii, E. Gheorghiu, Quality assessment of SPR sensor chips; case study on L1 chips, Biosens. Bioelectron. 45 (2013) 77–81.

[49] E. Hajjar, B. Korkmaz, F. Gauthier, B.O. Brandsdal, V. Witko-Sarsat, N. Reuter, Inspection of the binding sites of proteinase 3 for the design of a highly specific substrate, J. Med. Chem. 49 (2006) 1248–1260.
[50] S. Narawane, A. Bundjo, C. Grauffel, B.E. Haug, N. Reuter, In silico design, synthesis and assays of specific substrates for proteinase 3: influence of fluorogenic and charged groups, J. Med. Chem. 57 (2014) 1111–1115.
[51] E.M. Erb, X. Chen, S. Allen, C.J. Roberts, S.J. Tendler, M.C. Davies, S. Forsen, Characterization of the surfaces generated by liposome binding to the modified dextran matrix of a surface plasmon resonance sensor chip, Anal. Biochem. 280 (2000) 29–35.
[52] W. Cho, R.V. Stahelin, Membrane–protein interactions in cell signaling and membrane trafficking, Annu. Rev. Biophys. Biomol. Struct. 34 (2005) 119–151.
[53] S.H. White, W.C. Wimley, Hydrophobic interactions of peptides with membrane interfaces, Biochim. Biophys. Acta 1376 (1998) 339–352.
[54] W.C. Wimley, S.H. White, Experimentally determined hydrophobicity scale for proteins at membrane interfaces, Nat. Struct. Biol. 3 (1996) 842–848.
[55] S. Vanni, L. Vamparys, R. Gautier, G. Drin, C. Etchebest, P.F. Fuchs, B. Antonny, Amphipathic lipid packing sensor motifs: probing bilayer defects with hydrophobic residues, Biophys. J. 104 (2013) 575–584.
[56] G. van Meer, D.R. Voelker, G.W. Feigenson, Membrane lipids: where they are and how they behave, Nat. Rev. Mol. Cell Biol. 9 (2008) 112–124.
[57] D.L. Daleke, Regulation of transbilayer plasma membrane phospholipid asymmetry, J. Lipid Res. 44 (2003) 233–242.
[58] R.F.A. Zwaal, A.J. Schroit, Pathophysiologic implications of membrane phospholipid asymmetry in blood cells, Blood 89 (1997) 1121–1132.
[59] N. Hu, J. Westra, C.G. Kallenberg, Membrane-bound proteinase 3 and its receptors: relevance for the pathogenesis of Wegener's granulomatosis, Autoimmun. Rev. 8 (2009) 510–514.
[60] S. von Vietinghoff, G. Tunnemann, C. Eulenberg, M. Wellner, M.C. Cardoso, F.C. Luft, R. Kettritz, NB1 mediates surface expression of the ANCA antigen proteinase 3 on human neutrophils, Blood 109 (10) (2007) 4487–4493.
[61] A. David, R. Fridlich, I. Aviram, The presence of membrane proteinase 3 in neutrophil lipid rafts and its colocalization with FcgammaRIIIb and cytochrome b558, Exp. Cell Res. 308 (2005) 156–165.
[62] A. David, Y. Kacher, U. Specks, I. Aviram, Interaction of proteinase 3 with CD11b/CD18 (beta2 integrin) on the cell membrane of human neutrophils, J. Leukoc. Biol. 74 (2003) 551–557.
[63] B. Jiang, E. Grage-Griebenow, E. Csernok, K. Butherus, S. Ehlers, W.L. Gross, J.U. Holle, The role of proteinase 3 (PR3) and the protease-activated receptor-2 (PAR-2) pathway in dendritic cell (DC) maturation of human-DC-like monocytes and murine DC, Clin. Exp. Rheumatol. 28 (2010) 56–61.
[64] C.J. Kuckleburg, P.J. Newman, Neutrophil proteinase 3 acts on protease-activated receptor-2 to enhance vascular endothelial cell barrier function, Arterioscler. Thromb. Vasc. Biol. 33 (2013) 275–284.
[65] B. Korkmaz, A. Kuhl, B. Bayat, S. Santoso, D.E. Jenne, A hydrophobic patch on proteinase 3, the target of autoantibodies in Wegener granulomatosis, mediates membrane binding via NB1 receptors, J. Biol. Chem. 283 (2008) 35976–35982.
[66] C. Kantari, M. Pederzoli-Ribeil, O. Amir-Moazami, V. Gausson-Dorey, I.C. Moura, M.C. Lecomte, M. Benhamou, V. Witko-Sarsat, Proteinase 3, the Wegener autoantigen, is externalized during neutrophil apoptosis: evidence for a functional association with phospholipid scramblase 1 and interference with macrophage phagocytosis, Blood 110 (2007) 4086–4095.
[67] J. Gabillet, A. Millet, M. Pederzoli-Ribeil, P. Tacnet-Delorme, L. Guillevin, L. Mouthon, P. Frachet, V. Witko-Sarsat, Proteinase 3, the autoantigen in granulomatosis with polyangiitis, associates with calreticulin on apoptotic neutrophils, impairs macrophage phagocytosis, and promotes inflammation, J. Immunol. 189 (2012) 2574–2583.